Acta Crystallographica Section A
Foundations of Crystallography
ISSN 0108-7673

Received 15 October 2001
Accepted 22 January 2002

Wavefunctions derived from experiment. IV. Investigation of the crystal environment of ammonia

Ian Bytheway,[a] Daniel J. Grimwood,[a] Brian N. Figgis,[a] Graham S. Chandler[a] and Dylan Jayatilaka[a,b]*

[a]Chemistry, School of Biomedical and Chemical Sciences, The University of Western Australia, 35 Stirling Hwy, Crawley, WA 6009, Australia, and [b]Research School of Chemistry, Australian National University, Canberra, ACT 0200, Australia. Correspondence e-mail: dylan@crystal.uwa.edu.au

Constrained Hartree–Fock calculations have been performed to obtain wavefunctions that reproduce experimental X-ray structure-factor magnitudes for crystalline NH_3 to within the limits of experimental error. Different model densities using both a single molecule and clusters of NH_3 in the calculation of X-ray structure-factor magnitudes have been examined. The effects of the crystalline lattice on the experimental wavefunction of the NH_3 unit can be reproducibly recovered. The construction of structure-factor magnitudes based on normally distributed random perturbations of the experimental values has also been used to gauge the accuracy of integrated atomic properties obtained from the wavefunctions, the point at which the constraint procedure should be terminated, and the approximate error in the experimental $\sigma(\mathbf{k})$ values.

1. Introduction

Recent papers have described a method for obtaining constrained Hartree–Fock (CHF) wavefunctions using X-ray diffraction data (Jayatilaka, 1998; Jayatilaka & Grimwood, 2001). The procedure is based upon an algorithm which successively modifies the *ab initio* Hartree–Fock wavefunction until the calculated structure-factor magnitudes agree, to within experimental error, with those obtained from the X-ray diffraction experiment. This procedure was applied to experimental data for crystalline beryllium (Jayatilaka, 1998) and α-oxalic acid dihydrate (Grimwood & Jayatilaka, 2001). In the latter case, topological analysis (Bader, 1990) of the total charge density obtained from the CHF calculations was also analysed (Bytheway *et al.*, 2002).

In this work, the constrained Hartree–Fock procedure has been applied to experimental X-ray diffraction data for crystalline NH_3 (Boese *et al.*, 1997) with particular emphasis placed upon the effect of choosing different sized NH_3 model clusters which are then propagated to obtain an electron density from which the crystal structure-factor magnitudes are calculated. The purpose of this was to study in detail the effect of the crystal lattice on the charge density of an NH_3 unit in the crystal, and to see whether or not the CHF procedure can reproducibly recover such effects in the electron density from the experimental data. NH_3 was chosen for this purpose because of its relatively small size, which makes it possible to build clusters of NH_3 molecules for which *ab initio* wavefunctions of reasonable quality can be constructed using the CHF method.

2. Theoretical details

2.1. Wavefunction calculations

A complete description of the constrained Hartree–Fock (CHF) procedure has been given elsewhere (Jayatilaka, 1998; Jayatilaka & Grimwood, 2001). In this paper, we are concerned with the question of how quickly the density for the isolated NH_3 unit approaches that of the bulk crystal. Three different models have been used for this purpose:

$(NH_3)_1$: A single NH_3 molecule as defined in Fig. 1(*a*).

$(NH_3)_4$: A cluster of the four NH_3 molecules that constitute a unit cell in crystalline NH_3, as shown in Fig. 1(*b*). The density of the crystallographically unique NH_3 (involved in intermolecular hydrogen bonding with the three other NH_3 molecules in the unit cell) is extracted and propagated to produce the theoretical crystal density.

$(NH_3)_7$: A cluster of seven NH_3 molecules, comprising a central NH_3 surrounded by its six nearest-neighbour NH_3 molecules, as shown in Fig. 1(*c*). The density of the central NH_3, which is involved in intermolecular hydrogen bonding with each of the six other NH_3 molecules, is extracted and propagated to produce the theoretical crystal density.

In each of these models for NH_3, the charge density of a single NH_3 molecule was extracted from the total charge density of the cluster using a Mulliken partitioning scheme (Grimwood & Jayatilaka, 2001) and theoretical structure factors $F^c(\mathbf{k})$ obtained by propagation of this density throughout the crystal system followed by Fourier transformation (Chandler *et al.*, 1994). Such an approach allows for the

propagation of a molecular charge density that has been perturbed by the proximity of neighbouring molecules, as is the case in the crystalline environment.

The experimental unit-cell parameters, bond lengths and angles for crystalline NH_3 obtained by Boese *et al.* (1997) at 160 K were used throughout. The structure-factor magnitudes from this study (Boese, 1999) were used in both CHF calculations and in a least-squares multipole refinement (see §2.2). Prior to use, the experimental intensities were merged and averaged, corrected for absorption and Lorentz–polarization effects (Figgis *et al.*, 1998) and converted to $F^o(\mathbf{k})$. After averaging, 84 unique reflections were obtained [$\sin\theta/\lambda < 0.71$ Å^{-1}, $F^o(\mathbf{k}) > 3\sigma(\mathbf{k})$] and used in both the CHF calculations and multipole refinement. Secondary-extinction effects were accounted for by the Larson model (Larson, 1970) to minimize the χ^2 value. The Stewart model for basis function pairs was used to make the corrections for thermal motion (Stewart, 1969) during the CHF calculations in conjunction with the thermal parameters for model *M* of Boese *et al.* (1997): for N, $U_{11} = 0.0372$ and $U_{12} = -0.0009$ Å^2; for H, $U_{11} = 0.053$ Å^2.

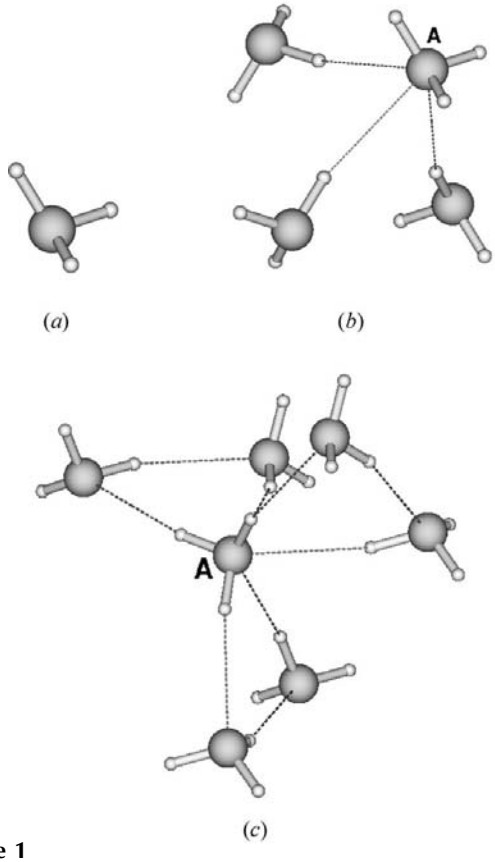

Figure 1
Schematic representations (Schaftenaar & Noordik, 2000) of the various NH_3 clusters used to generate theoretical structure-factor magnitudes. In all clusters, the X-ray diffraction values (Boese *et al.*, 1997) are used to define the arrangement of the NH_3 molecules: space group $P2_13$; unit-cell length 5.1305 Å, d(N—H) = 1.01 Å; ∠HNH = 109.1°, d(N···H) = 2.40 Å. (*a*) The single molecule of NH_3. (*b*) The unit-cell arrangement of NH_3 used to define the $(NH_3)_4$ cluster. (*c*) The $(NH_3)_7$ cluster. The propagated NH_3 molecule is marked *A* in (*b*) and (*c*).

All of the Hartree–Fock calculations described here, both conventional and constrained, were performed using the *TONTO* software package (Jayatilaka & Grimwood, 2000). The Pople 6-311G++ (2*d*, 2*p*) basis set (Krishnan *et al.*, 1980) was used throughout. Topological analyses of the total charge densities and the evaluation of integrated atomic properties based on partitioning of the total charge density were performed with the *MORPHY98* software (Popelier & Bone, 1998).

2.2. Multipole refinement of experimental data

The averaged data set described above was also subjected to least-squares refinement:

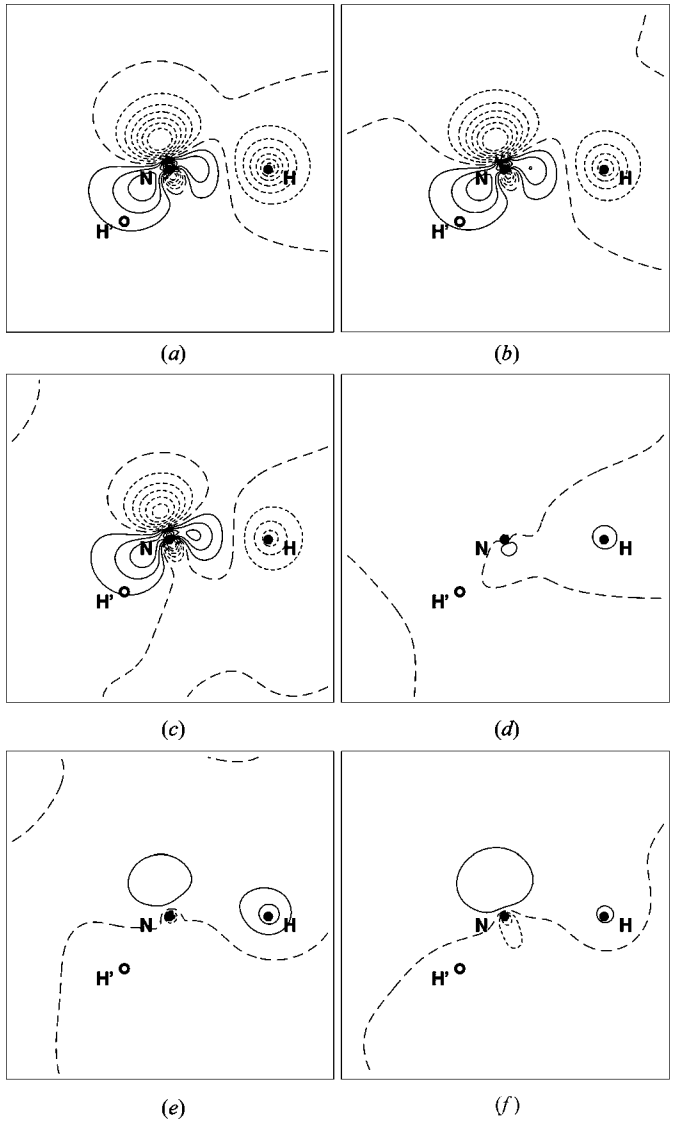

Figure 2
Maps of the differences in charge densities obtained from the various wavefunctions. Contours are in steps of 0.008 a.u: full lines denote contours of positive ρ, broken lines denote contours of negative ρ and the zero contour is denoted by a dashed line. (*a*) $\rho(NH_3)_{1,\chi^2=1.0} - \rho(NH_3)_{1,\chi^2=10.9}$. (*b*) $\rho(NH_3)_{4,\chi^2=1.0} - \rho(NH_3)_{1,\chi^2=10.9}$. (*c*) $\rho(NH_3)_{7,\chi^2=1.0} - \rho(NH_3)_{1,\chi^2=10.9}$. (*d*) $\rho(NH_3)_{4,\chi^2=1.0} - \rho(NH_3)_{1,\chi^2=1.0}$. (*e*) $\rho(NH_3)_{7,\chi^2=1.0} - \rho(NH_3)_{1,\chi^2=1.0}$. (*f*) $\rho(NH_3)_{7,\chi^2=1.0} - \rho(NH_3)_{4,\chi^2=1.0}$.

Table 1
Values of χ^2, the extinction coefficients and electronic energies obtained from the calculations using the various models to describe crystalline NH_3.

The column denoted HF refers to the value of χ^2 for a conventional molecular gas-phase Hartree–Fock calculation and the columns denoted CHF refer to constrained Hartree–Fock wavefunction calculations. The parameter λ denotes the value of the Lagrange multiplier required to produce the corresponding χ^2 for the CHF wavefunction.

	HF			CHF			
	χ^2	Extinction (10^{-5})	$-E$(HF) (Hartree)	λ (10^{-3})	χ^2	Extinction (10^{-5})	$-E$(CHF) (Hartree)
Experimental data							
$(NH_3)_1$	10.9	8.9	56.218023	6.5	1.0	9.5	56.206282
				4.5	1.4	9.6	56.208473
$(NH_3)_4$	11.3	9.6	224.876322	5.2	1.0	7.4	224.867871
$(NH_3)_7$	8.0	12.0	393.546519	3.75	1.0	1.7	393.541667
Random error data							
$(NH_3)_1$ (Set 1)	12.4	10.8	56.218023	100	1.3	17.8	56.186692
				4.2	2.8	11.0	56.208728
$(NH_3)_1$ (Set 2)	12.0	4.8	56.218023	3.25	2.7	4.3	56.210208

$$\sum w[F^o(\mathbf{k}) - k|F^c(\mathbf{k})|]^2 \quad (1)$$

using the Hansen–Coppens multipole formalism (Hansen & Coppens, 1978; Coppens, 1997) as implemented in the *XD* software (Koritsanszky *et al.*, 1997). The weighting scheme used was $w = \sigma^{-2}[F^o(\mathbf{k})]$ and only reflections with $F^o(\mathbf{k}) > 3\sigma(\mathbf{k})$ were used in the refinement. Electroneutrality of the NH_3 molecule was enforced throughout the refinement procedure.

The multipole refinement was carried out in three steps. In the first, multipole functions with $l \leq 4$ for the nitrogen atom ($M1$, $D0$, $Q0$, $O0$, $O3\pm$, $H0$, $H3\pm$) and $l \leq 2$ for hydrogen atoms ($M1$, $D0$, $D1\pm$, $Q0$, $Q1\pm$, $Q2\pm$) were refined. The κ and κ' parameters, which control the radial extent of the spherical and aspherical density, respectively, were then refined while the multipole populations remained fixed at the values obtained from the first stage of refinement. Both κ and κ' for the hydrogen atom were fixed throughout at 1.2 (Boese *et al.*, 1997; Koritsanszky *et al.*, 2000).

In the final refinement stage, the multipole functions κ(N) and κ'(N) were refined together, after which κ(N) and κ'(N) were 0.91 and 0.92, respectively. The monopole populations M(N) and M(H) were 2.04 and 0.63, respectively, and agreement statistics after this final refinement cycle were: $R = 0.0102$; $R_w = 0.0084$; GOF = 0.95 and $\chi^2 = 0.90$.

The topology of the total charge density derived from multipole refinement was analysed and these results are denoted in subsequent tables and discussion by $(NH_3)_{XD}$. Virial partitioning of the total charge density was performed with the *TOPXD* software (Volkov *et al.*, 2000).

2.3. Crystalline molecular-orbital calculations

Ab initio Hartree–Fock calculations for crystalline NH_3 utilizing the crystalline molecular orbital (CMO) method were performed with the *CRYSTAL98* software (Saunders *et al.*, 1998). The experimental (Boese *et al.*, 1997) cell parameters used in the CHF calculations and multipole refinements described above were also used in the periodic HF calculations. The extended basis sets used in the molecular calculations were not appropriate for the CMO calculations, and instead the double-ζ basis sets of Thakkar *et al.* (1993) were used after a recent study (Spackman & Mitchell, 2001) showed that these basis sets are suitable for periodic *ab initio* calculations. The Monkhorst shrinking factor was set to 8, which yielded a total of 45k points in the irreducible Brillouin zone (Saunders *et al.*, 1998). The total charge density from the periodic Hartree–Fock calculation was analysed with the *TOPOND98* software (Gatti, 1998) and the results denoted in subsequent tables and discussion by $(NH_3)_{CMO}$.

3. The effect of molecular environment on constrained wavefunction calculations

χ^2, extinction coefficients, λ and electronic energies obtained from the various wavefunctions of NH_3 are given in Table 1. The extinction coefficients in Table 1 reflect the variety of $F^c(\mathbf{k})$ and $F^o(\mathbf{k})$ used in the HF and CHF calculations (Jayatilaka & Grimwood, 2001), while the electronic energies of the CHF wavefunctions reflect the energy penalty, of the order of 12–80 kJ mol^{-1}, required to obtain the desired agreement with experiment. The first column of χ^2 values in Table 1 shows the agreement between the experimental structure-factor magnitudes and those obtained prior to performing the constrained wavefunction, *i.e.* when $\lambda = 0$. These χ^2 show that the cluster of seven NH_3 molecules, from which the central molecule was used to obtain $F^c(\mathbf{k})$, gives the best agreement with experiment. This is clear evidence that the $(NH_3)_7$ model cluster is a better match with experiment than a calculation for a single, isolated molecule. The difference between the $(NH_3)_7$ and $(NH_3)_4$ models is also clear: prior to the application of the Lagrangian constraint, the $(NH_3)_4$ (unit cell) cluster of NH_3 molecules does not result in $F^c(\mathbf{k})$ that agree better with experiment than those obtained from the use of a single NH_3 molecule.

Difference density plots comparing the various total charge-density $\rho(\mathbf{r})$ distributions are shown in Fig. 2. Comparison of the $(NH_3)_{1,\chi^2=1.0}$ and $(NH_3)_{1,\chi^2=10.9}$ total charge densities (Fig. 2*a*) shows a reduction of charge in the lone-pair region of the N atom, a slight increase in charge density in the region near the N nucleus, and a decrease in the region near the H nucleus.

Table 2
Topological properties derived from analysis of the various total charge densities.

$(NH_3)_1$, $(NH_3)_4$ and $(NH_3)_7$ denote the cluster model used to obtain the CHF wavefunction, $(NH_3)_{CMO}$ denotes properties derived from the crystalline molecular-orbital calculation, and $(NH_3)_{XD}$ denotes the properties derived from multipole refinement of the experimental structure factors. χ^2 is the agreement statistic between the experimental structure factors and those obtained from the various models and methods. $\rho(\mathbf{r}_b)$ and $\nabla^2\rho(\mathbf{r}_b)$ are the values of the charge density and its Laplacian at the bond critical point, and d(N) denotes the distance from the nitrogen nucleus to the bond critical point. The properties obtained from integration of the atoms defined by the zero-flux surfaces in the total charge density are: the atomic charge q(N) and q(H); the atomic kinetic energy K(N) and K(H); the atomic volume v(N) and v(H); the magnitude of the atomic dipole moment $|\mathbf{M}(N)|$ and $|\mathbf{M}(H)|$. Values of the (3, −3) critical points in L for the valence shell of nitrogen are also given: L(nb) corresponds to the value of L for the non-bonding or lone-pair charge concentration maximum; L(bo) corresponds to the value of L for the three bonding charge concentration maxima; d(bo) and d(nb) are the distances from the nitrogen nucleus to the respective charge concentration maxima. All values are in atomic units.

	$(NH_3)_1$		$(NH_3)_4$		$(NH_3)_7$		$(NH_3)_{CMO}$	$(NH_3)_{XD}$
χ^2	10.9	1.0	11.3	1.0	8.0	1.0		0.9
N—H bond								
$\rho(\mathbf{r}_b)$	0.35	0.33	0.35	0.34	0.35	0.34	0.35	0.30
$-\nabla^2\rho(\mathbf{r}_b)$	1.77	2.13	1.80	2.06	1.86	2.03	1.87	1.16
d(N)	1.395	1.485	1.400	1.467	1.411	1.457	1.432	1.503
N···H bond								
$\rho(\mathbf{r}_b)$	–	–	0.01	0.01	0.01	0.01	0.01	0.01
$\nabla^2\rho(\mathbf{r}_b)$	–	–	0.04	0.04	0.04	0.04	0.04	0.04
d(N)	–	–	2.860	2.875	2.880	2.888	2.878	2.960
Integrated properties								
$-q$(N)	1.05	1.53	1.08	1.43	1.18	1.42	1.24	1.50
q(H)	0.35	0.51	0.37	0.49	0.39	0.47	0.41	0.50
K(N)	54.6755	54.9866	54.7210	54.9357	54.7687	54.9200	54.8187	–
K(H)	0.4832	0.3666	0.4758	0.3882	0.4651	0.4037	0.4529	–
v(N)	138.7	162.6	124.4	139.3	128.0	138.0	138.0	153.8
v(H)	32.3	26.5	31.6	27.2	27.5	24.6	26.7	24.0
$\|\mathbf{M}(N)\|$	0.16	0.13	0.11	0.07	0.14	0.02	0.13	0.33
$\|\mathbf{M}(H)\|$	0.18	0.18	0.17	0.18	0.16	0.16	0.16	0.18
Atomic graph of N								
L(nb)	2.65	1.90	2.61	2.00	2.46	2.05	2.23	2.83
d(nb)	0.748	0.764	0.740	0.766	0.756	0.766	0.751	0.785
L(bo)	2.13	2.19	2.15	2.20	2.19	2.21	1.82	3.52
d(bo)	0.831	0.822	0.830	0.823	0.828	0.823	0.881	0.775

Similar comparison of the $(NH_3)_{4,\chi^2=1.0}$ and $(NH_3)_{7,\chi^2=1.0}$ densities with the $(NH_3)_{1,\chi^2=10.9}$ charge density show similar features (Figs. 2*b* and *c*). Difference density plots obtained from comparison of the three constrained wavefunction calculations are, on the other hand, almost featureless (Figs. 2*d*, *e* and *f*). From a visual perspective, these densities are essentially identical, indicating that the use of experimental $F^c(\mathbf{k})$ overcomes the differences in these models that are apparent prior to the CHF calculation.

4. N—H and N···H bonding

Table 2 shows results obtained from an atoms in molecules (AIM) (Bader, 1990) analysis of the different constrained and unconstrained wavefunctions, together with those from the CMO calculations and multipole refinement. Values of the charge density at the NH bond critical point [$\rho(\mathbf{r}_b)$] obtained from the CHF wavefunctions show only a slight decrease (3–5%) when compared with the unconstrained quantity, and results from the CMO and XD studies are close to the *ab initio* values, with the latter being slightly smaller. As was also noted in our preceding study of α-oxalic acid dihydrate (Bytheway *et al.*, 2002), the value of the Laplacian of the charge density at the bond critical point [$\nabla^2\rho(\mathbf{r}_b)$] shows variability between the different calculations. The distance from the bond critical point to the nitrogen nucleus, d(N), increases after wavefunction constraint; the change is largest for the $(NH_3)_1$ model (0.09 a.u.) and least for the $(NH_3)_7$ model (0.046 a.u.). The value of d(N) from the CMO calculation is between the constrained and unconstrained values, while the multipole-derived value of d(N) is larger, and closer to the constrained wavefunction values.

Bond critical-point data corresponding to the N···H hydrogen bond show remarkable similarity for all of the calculations. All predict a value of 0.1 a.u. for the value of $\rho(\mathbf{r}_b)$ and 0.04 a.u. for $\nabla^2\rho(\mathbf{r}_b)$ irrespective of the method used to obtain the total charge density. The distance between the N···H bond critical point and the nitrogen nucleus does, however, show variation amongst the methods. There is an increase in this distance on going from the unconstrained to constrained charge densities for both the $(NH_3)_4$ and $(NH_3)_7$ model densities, and these CHF values are similar to those obtained from the $(NH_3)_{CMO}$ and $(NH_3)_{XD}$ results. This is consistent with the finding that for all of the NH_3 model clusters the electron population of the nitrogen atom increases (see the next section) on going from the unconstrained to the constrained wavefunction.

5. Integrated atomic properties

Charges obtained by integrating over the atomic basins defined by the zero-flux surfaces for each atom (Bader, 1990)

are markedly different on going from the molecular charge density of the single NH_3 molecule in the gas phase to those obtained from the constrained wavefunctions. The net charge obtained for nitrogen, q(N), from the $(NH_3)_{1,\chi^2=10.9}$ wavefunction is -1.05 e while the values obtained from the constrained wavefunctions show an increase in the net electron population of nitrogen. Net charges on hydrogen vary accordingly. The change in electron populations on going from an isolated NH_3 molecule to one involved in crystal packing is also supported by the CMO calculation and multipole refinement. In both of these treatments of NH_3, the degree of charge separation is also larger than was found in the gas-phase calculations.

The remarks in the preceding paragraph are in accord with the results of an earlier *ab initio* study of crystalline ammonia which also noted an increase in the polarity of the N—H bond on going from the gas to the crystalline phase (Taurian & Lunell, 1987). This difference is a consequence of the packing of NH_3 molecules in the crystal lattice: each N atom is involved in three intermolecular hydrogen bonds, and correspondingly each H atom is involved in an intermolecular hydrogen bond. The change in q(H) as a result of intermolecular hydrogen-bond formation was also noted in our previous study of α-oxalic acid dihydrate where q(H) is larger for the hydrogen atom involved in hydrogen bonding to an oxygen atom (Bytheway *et al.*, 2002) than for that not so bonded.

It is also worth pointing out that the change in atomic charges indicate that the intermolecular hydrogen-bonding interactions are accounted for during the constrained wavefunction calculation that used the $(NH_3)_1$ model. The q(N) obtained from the $(NH_3)_{1,\chi^2=1.0}$ wavefunction more closely resembles both the $(NH_3)_{4,\chi^2=1.0}$ and $(NH_3)_{7,\chi^2=1.0}$ values than the gas-phase $(NH_3)_{1,\chi^2=10.9}$ value. This finding is consistent with the plots in Fig. 2 and provides further evidence that in the present study the experimental data inform the theoretical procedure to produce a consistent wavefunction representing experiment.

The atomic kinetic energies, K(N) and K(H) in Table 2, also reflect the increased charge transfer from hydrogen to nitrogen in the crystalline systems. In particular, the change in K(H) on going from the gas phase to the CHF wavefunction indicates the destabilization of the hydrogen atom, which is typical of hydrogen-bond formation (Popelier & Bader, 1992; Popelier & Koch, 1995; Popelier, 1998).

The decrease in atomic volume of H, v(H) in Table 2, on going from the isolated to the crystalline molecule is also consistent with the formation of intermolecular hydrogen bonding and the presence of other NH_3 molecules in the crystal lattice. The CHF values of v(H) show a decrease in volume of the order of 20%, which is also consistent with v(H) obtained from the CMO calculation. The value of v(N) changes much less over the range of calculations, with the exception of the value obtained from the CHF wavefunction for $(NH_3)_{1,\chi^2=1.0}$, which increased by approximately 17% with respect to the gas-phase value. This result, along with the value of v(N) from the CMO calculation which is similar to the CHF values obtained for the $(NH_3)_{4,\chi^2=1.0}$ and $(NH_3)_{7,\chi^2=1.0}$ calculations, suggests slight expansion of the atomic envelope of N in the absence of the other lattice NH_3 molecules in the CHF calculation.

The values of $|\mathbf{M}(\mathrm{N})|$ for $(NH_3)_{4,\chi^2=1.0}$ and $(NH_3)_{7,\chi^2=1.0}$ are smaller than the $(NH_3)_{1,\chi^2=10.9}$, $(NH_3)_{\mathrm{CMO}}$ and $(NH_3)_{\mathrm{XD}}$ results. Despite the differences encountered for $|\mathbf{M}(\mathrm{N})|$, values of $|\mathbf{M}(\mathrm{H})|$ are all quite similar.

6. The bonding and lone-pair electrons of nitrogen

The Laplacian of the charge density, $L = -\nabla^2\rho(\mathbf{r})$, shows regions where charge is locally concentrated or depleted, (Bader *et al.*, 1988; Bader, 1990) and is useful for probing the differences between the various wavefunctions. Each of the calculations yielded $(3, -3)$ critical points in L that can be thought of as the 'non-bonding' (nb) and 'bonding' (bo) pairs of electrons in the valence shell of nitrogen in NH_3. Values of the $(3, -3)$ critical points in L in the valence shell of the nitrogen atom, as well as their distance from the nucleus, are given in Table 2.

The bonding charge concentration maxima are further from the nitrogen nucleus than the non-bonding maximum, as anticipated by valence-shell electron repulsion (vsepr) arguments (Gillespie & Hargittai, 1991). An unexpected result perhaps is the difference in the values of L at these maxima, as the value obtained for the non-bonded maxima from the three CHF charge densities, as well as the multipole-fitted density, are all *smaller* than the bonding maxima. The situation is reversed for the gas-phase and CMO calculations where the larger value of the charge concentration belongs to the non-bonded maximum.

7. Estimating errors in constrained wavefunction calculations

7.1. The accuracy of atomic properties

The atomic properties presented above contain errors due to the imprecise experimental determination of the structure factors. In the estimation of such errors, we are, of course, reliant upon the accuracy of the $\sigma(\mathbf{k})$ value associated with each measured structure factor, because it is these errors that are used to decide when the constraint procedure should be terminated: namely when χ^2 is unity. Clearly, the veracity of subtle distinctions between fitted and unfitted wavefunctions require accurate data since large $\sigma(\mathbf{k})$ would result in $\chi^2 = 1$ with the application of only a modest constraint.

In order to examine the effects of these errors, a new data set was constructed by adding to the experimental data a normally distributed error with standard deviation $\sigma(\mathbf{k})$ using the algorithm described in the preceding paper (Bytheway *et al.*, 2002). These 'random-error' structure factors are denoted Set 1.

Initial application of the CHF procedure to these random-error data, and using the $(NH_3)_1$ model, resulted in a wavefunction with a χ^2 value of 1.4. There was no possibility of

Table 3
Properties calculated from analysis of the total charge-density distributions obtained from refinement of random error data sets, compared with a CHF wavefunction with $\chi^2 = 1.4$ using the experimental data.

The symbols have the same definitions as those given in Table 2 and all values are in atomic units.

		Random error data			
		Set 1			Set 2
	Exp. data				
	CHF	CHF		XD	CHF
χ^2	1.4	2.8	1.4	2.5	2.8
N—H bond					
$\rho(\mathbf{r}_b)$	0.33	0.33	0.33	0.30	0.34
$-\nabla^2\rho(\mathbf{r}_b)$	2.09	2.09	2.40	1.18	2.04
d(N)	1.475	1.473	1.539	1.509	1.465
Integrated properties					
$-q$(N)	1.48	1.47	1.80	1.53	1.43
q(H)	0.49	0.49	0.60	0.51	0.48
K(N)	54.9570	54.9491	55.1609	–	54.9237
K(H)	0.3780	0.3811	0.3118	–	0.3909
v(N)	160.0	159.5	172.1	154.0	157.4
v(H)	27.2	27.3	21.8	23.6	27.9
$\lvert\mathbf{M}(\mathrm{N})\rvert$	0.10	0.10	0.43	0.35	0.08
$\lvert\mathbf{M}(\mathrm{H})\rvert$	0.18	0.18	0.17	0.18	0.18
Atomic graph of N					
L(nb)	1.96	1.96	2.05	2.26	2.06
d(nb)	0.765	0.765	0.768	0.795	0.762
L(bo)	2.19	2.19	2.22	3.04	2.17
				d(bo)	0.823

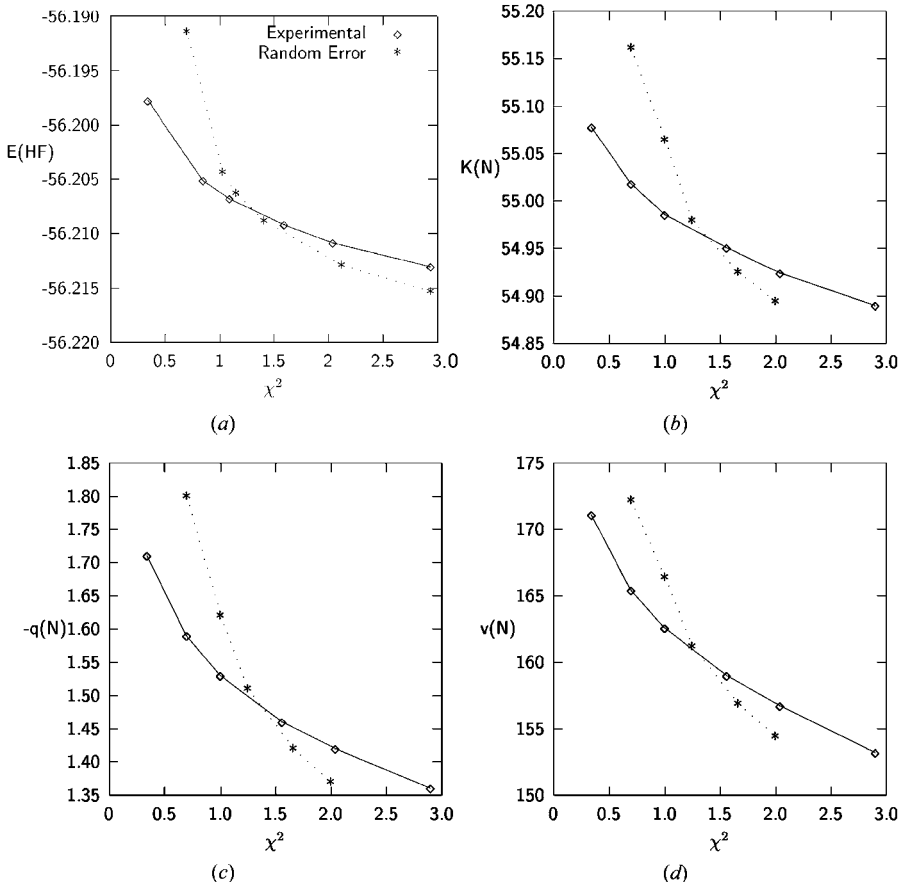

Figure 3
Plots of (*a*) the total HF energy E(HF), (*b*) the atomic kinetic energy of nitrogen K(N), (*c*) integrated atomic charge of nitrogen $-q$(N) and (*d*) atomic volume v(N) *versus* χ^2 for the experimental and random error (Set 1) data sets. χ^2 values for the random-error wavefunctions were halved prior to plotting. All values are in atomic units.

obtaining a $\chi^2 = 1.0$ since the change in χ^2 with increasing λ resulted in extremely slow convergence of the CHF procedure. In our previous work (Bytheway *et al.*, 2002), we also found that the χ^2 value of the random-error CHF wavefunction was larger than the χ^2 for the CHF wavefunction that used the original experimental data although the atomic properties from these oxalic acid wavefunctions were similar. By contrast, in the case of NH_3 studied here, the integrated atomic properties from the random error, $\chi^2 = 1.4$ wavefunction (Table 3) show marked differences when compared with the CHF wavefunction for the original experimental data (Table 2). For example, atomic charges differ by almost 18% and K(N) by over 400 kJ mol^{-1}. This is, of course, an unacceptable outcome.

7.2. Further investigation of the errors in atomic properties: estimating the accuracy of σ(k)

In order to investigate the origins of this discrepancy, a multipole refinement of the Set 1 data was performed using the procedure described in §2.2. The integrated atomic properties were in accord with those obtained from

refinement of the original experimental data. Namely, most properties are within 5% of each other. The agreement statistics for the multipole refinement of the random-error (Set 1) data are: $R = 0.0164$; $R_w = 0.0139$; GOF = 1.57; $\chi^2 = 2.5$. The R-factor agreements are only slightly worse than those obtained in the original refinement. The most interesting result, though, is that the value of χ^2 could not be refined any lower than about twice the value of that obtained from refinement of the original experimental data.

This observation is, in fact, a manifestation of a more general result: that application of the random-error algorithm to $F^o(\mathbf{k})$ requires that the $\sigma^2(\mathbf{k})$ values be doubled. That is, adding Gaussian noise with variance $\sigma^2(\mathbf{k})$ to data that are already noisy with variance $\sigma^2(\mathbf{k})$ results in data with variance $2\sigma^2(\mathbf{k})$ – provided it is assumed that the errors are independent (Applebaum, 1996). The end-point for the CHF procedure when applied to random-error data is, therefore, when χ^2 is 2, not unity.

If we assume that the estimates for $\sigma(\mathbf{k})$ are correct, the properties from the $\chi^2(\text{obs.}) = 1$ wavefunction should be compared to the properties from the $\chi^2(\text{Set 1}) = 2$ wavefunction. Any under- or overestimation in the $\sigma(\mathbf{k})$ values will result in another value of $\chi^2(\text{obs.})$, say $\chi^2(\text{obs.}) = \alpha$, where properties will be comparable with a random-error wavefunction with $\chi^2(\text{Set 1}) = 2\alpha$. In other words, this provides a means of probing the accuracy of the experimental $\sigma(\mathbf{k})$ values by comparison of properties from the observed and random-error wavefunctions.

To examine the accuracy of the $\sigma(\mathbf{k})$ for NH_3, plots of the relationship between various properties (total HF energy, integrated atomic kinetic energy, charge and volume) and the χ^2 value of the wavefunction used to obtain them was examined. Fig. 3 shows how atomic properties for the nitrogen atom vary over the range of χ^2 for the experimental data, and $\chi^2/2$ for the random-error data. If the $\sigma(\mathbf{k})$ values were correct, then the curves in these plots should, on the basis of the above argument, cross at χ^2 of 1. It is obvious, however, that the plots of atomic kinetic energy, charge and volume against χ^2 all produce curves that intersect at a χ^2 of about 1.4 and not unity. Since it is quite unlikely that four different properties would all intersect at roughly the same point in this manner, the consequences are twofold:

(i) the error in the $\sigma(\mathbf{k})$ for this data set is of the order of 15–20%;

(ii) the properties from the random-error CHF wavefunction with $\chi^2 = 2.8$ should be compared with the properties from the experimental CHF wavefunction with $\chi^2 = 1.40$.

Analyses of the wavefunctions obtained from CHF wavefunctions constrained to give χ^2 of 1.4 (experimental) and 2.8 (Set 1) are also shown in Table 3. The properties obtained from these two wavefunctions show the expected agreement and differences are of the order of 5% anticipated from our findings in the preceding paper (Bytheway *et al.*, 2002) and differences in K(N) are of the order of 20 kJ mol^{-1}.

These ideas were tested further by constructing another random-error data set, denoted Set 2, and subjecting it to the CHF procedure to obtain a wavefunction with a χ^2 of about 2.8. Table 3 shows properties obtained from this wavefunction, all of which agree with those obtained from the $\chi^2(\text{obs.}) = 1.4$ and $\chi^2(\text{Set 1}) = 2.8$ wavefunctions. It should be kept in mind, however, that the intersections shown in Fig. 3 represent an approximate value where the family of random-error curves would intersect the experimental curve. Hence the value of 2.80 for χ^2 is approximate, as curves similar to those shown in Fig. 3 were not constructed for the Set 2 data.

7.3. Comparison of plots of the χ^2 = 1.0 and χ^2 = 1.4 electron densities for $(NH_3)_1$

The results of the CHF calculations performed for the random-error data suggest that our original decision to terminate the procedure at a χ^2 of unity may have been erroneous. A plot of the difference density obtained from the $\chi^2(\text{obs.}) = 1.0$ and $\chi^2(\text{obs.}) = 1.4$ given in Fig. 4, however, shows that the two charge densities are essentially the same, at least upon visual inspection. The property plots in Fig. 3 show more clearly the differences between the two wavefunctions, which are small. Nevertheless, such plots provide a more sensitive measure of the differences between the wavefunctions than visual inspection of differences in the total charge density. The differences between the $\chi^2(\text{obs.}) = 1.0$ and $\chi^2(\text{obs.}) = 1.4$ wavefunctions are small and the original decision to terminate at $\chi^2(\text{obs.}) = 1.0$ was justified.

8. Conclusions

A procedure that allows modification of a Hartree–Fock wavefunction subject to the proviso that it produce structure factors in concordance with those obtained from experiment has been applied to the X-ray data obtained for the ammonia molecule. Analysis of the total charge density for this *experimental* wavefunction gave bond critical point values slightly larger than, though in general agreement with, those obtained previously using a multipole-fitting approach to the X-ray data (Boese *et al.*, 1997).

Comparison with theoretical *ab initio* calculations showed some interesting differences. Values of $\rho(\mathbf{r}_b)$(N—H) for both

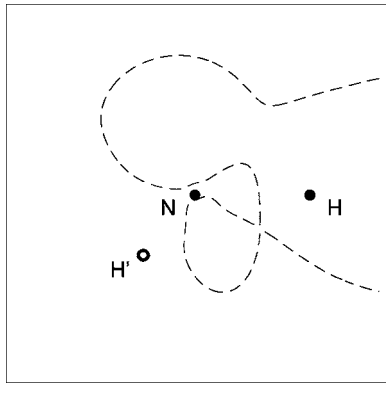

Figure 4
A plot of the difference density $\rho(NH_3)_{1,\chi^2=1.0} - \rho(NH_3)_{1,\chi^2=1.4}$. Plotting conventions are the same as those used in Fig. 2.

an isolated molecule and the crystalline phase were slightly larger than those obtained for the fitted wavefunction. Values of integrated atomic charges obtained from the three different constrained wavefunctions showed a larger degree of charge separation between the nitrogen and hydrogen atoms compared with the gas-phase values. Refinement of the experimental data using multipole density functions yielded similar integrated atomic charges to the constrained wavefunction values, as did the CMO calculations.

Analysis of the Laplacian of the charge density (L) showed the expected arrangement of three charge concentration maxima along N—H bonds and a single non-bonded charge concentration in the region usually attributed to the stereochemically active lone pair of electrons. An unexpected result was the change in the sizes of these bonding and non-bonding maxima in L. The charge densities obtained from the constrained wavefunctions and the multipole refinement of the experimental data gave a value of L at the position of the non-bonding maximum smaller than that at the bonding maximum, in contrast to the unconstrained and CMO charge densities.

Previous techniques for estimating the errors in atomic properties, which were adequate for α-oxalic acid dihydrate, have proved inadequate for the ammonia crystal. In this paper, we have described a procedure where the usual prediction of properties has been inverted, in a manner which provides an estimate of the errors in the experimental $\sigma(\mathbf{k})$ values. The new method uses experimental data to which Gaussian noise was added – so-called random-error data. Properties from two CHF wavefunctions, one constrained to experimental and the other to random-error data, are compared in order to extract the point at which the properties best agree. According to this method, the $\sigma(\mathbf{k})$ values were 15–20% in error and a $\chi^2 = 1.4$ is an appropriate value at which the CHF procedure using these experimental data should be terminated. Despite the fact that the $\sigma(\mathbf{k})$ values are in error, the properties obtained from the $\chi^2 = 1.0$ and $\chi^2 = 1.4$ CHF wavefunctions are almost identical, as is the total charge density.

In summary, the approach to the interpretation of experimental data described in this paper is an attempt to incorporate the results of experiment with the methods typically used in theoretical chemistry. It allows for a ready transferral of the methods routinely applied in contemporary *ab initio* calculations to the data obtained from X-ray diffraction experiments.

We thank Professor R. Boese for the experimental data for NH_3; Dr Carlo Gatti for the *TOPOND* software; and Drs A. Volkov, C. Gatti, Yu. Abramov and Professor P. Coppens for the *TOPXD* software. Financial support from the Australian Research Council is gratefully acknowledged.

References

Applebaum, D. (1996). *Probability and Information: an Integrated Approach.* Cambridge University Press.
Bader, R. F. W. (1990). *Atoms in Molecules: a Quantum Theory.* Oxford University Press.
Bader, R. F. W., MacDougall, P. J. & Gillespie, R. J. (1988). *J. Am. Chem. Soc.* **110**, 7329–7336.
Boese, R. (1999). Private communication.
Boese, R., Niederprüm, N., Bläser, D., Maulitz, A., Antipin, M. & Mallinson, P. R. (1997). *J. Phys. Chem.* B**101**, 5794–5799.
Bytheway, I., Grimwood, D. J. & Jayatilaka, D. (2002). *Acta Cryst.* A**58**, 232–243.
Chandler, G. S., Figgis, B. N., Reynolds, P. A. & Wolff, S. K. (1994). *Chem. Phys. Lett.* **225**, 421–426.
Coppens, P. (1997). *X-ray Charge Densities and Chemical Bonding.* Oxford University Press.
Figgis, B. N., Sobolev, A. N., Young, D. M., Schultz, A. J. & Reynolds, P. A. (1998). *J. Am. Chem. Soc.* **120**, 8715–8723.
Gatti, C. (1998). *TOPOND.* CNR–CSRSRC, Milan, Italy.
Gillespie, R. J. & Hargittai, I. (1991). *The VSEPR Model of Molecular Geometry.* Boston: Allyn and Bacon.
Grimwood, D. J. & Jayatilaka, D. (2001). *Acta Cryst.* A**57**, 87–100.
Hansen, N. K. & Coppens, P. (1978). *Acta Cryst.* A**34**, 909–921.
Jayatilaka, D. (1998). *Phys. Rev. Lett.* **80**, 798–801.
Jayatilaka, D. & Grimwood, D. J. (2000). *Tonto: a Research Tool for Quantum Chemistry.* The University of Western Australia, Nedlands, Western Australia, Australia.
Jayatilaka, D. & Grimwood, D. J. (2001). *Acta Cryst.* A**57**, 76–86.
Koritsanszky, T., Howard, S. T., Su, Z., Mallinson, P. R., Richter, T. & Hansen, N. (1997). *XD, Computer Program Package for Multipole Refinement and Analysis of Electron Densities from Diffraction Data.* Free University of Berlin, Berlin, Germany.
Koritsanszky, T., Zobel, D. & Luger, P. (2000). *J. Phys. Chem.* A**104**, 1549–1556.
Krishnan, R., Binkley, J. S., Seeger, R. & Pople, J. A. (1980). *J. Chem. Phys.* **72**, 650–654.
Larson, A. C. (1970). *Crystallographic Computing Techniques*, edited by F. R. Ahmed, pp. 291–294. Munksgaard: Copenhagen.
Popelier, P. L. A. (1998). *J. Phys. Chem.* A**102**, 1873–1878.
Popelier, P. L. A. & Bader, R. F. W. (1992). *Chem. Phys. Lett.* **189**, 542–548.
Popelier, P. L. A. & Bone, R. G. A. (1998). *MORPHY98.* UMIST, Manchester, England.
Popelier, P. L. A. & Koch, U. (1995). *J. Phys. Chem.* A**99**, 9747–9754.
Saunders, V. R., Dovesi, R., Roetti, C., Causà, M., Harrison, N. M., Orlando, R. & Zicovich-Wilson, C. M. (1998). *CRYSTAL 98 Users Manual.* University of Torino, Torino, Italy.
Schaftenaar, G. & Noordik, J. H. (2000). *J. Comput. Aided Mol. Design*, **14**, 123–134.
Spackman, M. A. & Mitchell, A. S. (2001). *Phys. Chem. Chem. Phys.* **3**, 1518–1523.
Stewart, R. F. (1960). *J. Chem. Phys.* **51**, 4569–4577.
Taurian, O. E. & Lunell, S. (1987). *J. Phys. Chem.* **91**, 2249–2253.
Thakkar, A. J., Koga, T., Saito, M. & Hoffmeyer, R. E. (1993). *Int. J. Quantum Chem. Quantum Chem. Symp.* **27**, 343–354.
Volkov, A., Gatti, C., Abramov, Y. & Coppens, P. (2000). *Acta Cryst.* A**56**, 252–258.